1995MNRAS.275..417D

Mon. Not. R. Astron. Soc. **275,** 417–428 (1995)

The complex variable soft X-ray spectrum of NGC 5548

C. Done,[1]★ K. A. Pounds,[1] K. Nandra[2] and A. C. Fabian[2]

[1] *Department of Physics and Astronomy, University of Leicester, University Road, Leicester LE1 7RH*
[2] *Institute of Astronomy, Madingley Road, Cambridge CB3 0HA*

Accepted 1995 February 3. Received 1995 February 1; in original form 1994 October 13

ABSTRACT

We present *ROSAT* 0.2–2 keV monitoring data on NGC 5548 taken over the period 1992 December–1993 January, when the source was at its historical maximum in X-ray flux. The data show a soft excess and partially ionized absorber modifying the high-energy power-law ($\alpha \sim 0.9$) spectrum. The major variability during the campaign is a strong flare event over 8 d, in which the soft excess brightens *without* a corresponding change in the power-law intensity. This is incompatible with the simple reprocessing models which are currently popular, where the soft excess is produced from thermalized hard X-ray emission illuminating an accretion disc. Given the high source luminosity, $\geq 0.1\ L_{\rm Edd}$, it seems likely that the soft excess is dominated by intrinsic emission from the accreting material.

While the data do not allow the ionization of the absorbing material to be constrained in each single spectrum, a comparison of the brightest spectrum with that from a long exposure taken 2 d later and which is a factor of 2 fainter shows a significant decrease in the ionization. This implies a density of $\geq 5 \times 10^5\ {\rm cm}^{-3}$ for the warm material, and hence a distance of less than $\sim 10^{18}$ cm from the central source.

Key words: accretion, accretion discs – galaxies: active – galaxies: individual: NGC 5548 – X-rays: galaxies.

1 INTRODUCTION

NGC 5548 is one of the best-studied, low-luminosity AGN, being bright and variable in the optical, UV and X-rays. It has been the subject of several monitoring campaigns to study the geometry of the broad-line region (BLR) through the lagged and smeared response of the lines to continuum variability (Clavel et al. 1991). These campaigns have been successful in showing clear stratification of the BLR (Krolik et al. 1991). Perhaps the most unexpected result has been the behaviour of the continuum flux, with correlated variability between the optical and UV with no lag greater than the 4-d observation spacing. This is in direct conflict with the predictions of continuum variability from a viscous accretion disc, where the (long) sound-crossing time-scale determines the differential response of the smaller radius UV emission region compared with the optical. Despite the relative success of viscous accretion discs in explaining the 'big blue bump' spectra (e.g. Laor 1990), this correlated variability unambiguously rules out such models, and suggests that the optical and UV emission are mainly produced by reprocessing of higher energy flux, so that changes occur on the (short) light-travel time. The most popular of these models has the accretion disc as the reprocessor of the radiation (Krolik et al. 1991; Clavel et al. 1992; Ross & Fabian 1993), but the cool material could also be in the form of many small clouds surrounding the X-ray source (Guilbert & Rees 1988; Celotti, Fabian & Rees 1992; Barvainis 1993).

Coincident with these developments, *Ginga* data have given a substantial insight into the 2–20 keV X-ray spectra of Seyfert 1 AGN. The discovery of spectral features, most notably the iron Kα fluorescent line, iron K absorption edge, and a high-energy excess in the data, indicated that the X-ray source illuminates substantial amounts of both partially ionized and neutral material (see, e.g., the review by Mushotzky, Done & Pounds 1993, and references therein). The former is the 'warm absorber', tentatively identified with the scattering region required in Seyfert unification schemes (see, e.g., the review by Antonucci 1993, and references therein). This material is thought to be an outflowing wind, perhaps from the irradiated molecular torus (Krolik & Begelman 1986), which is partially ionized by the intense X-ray flux and imprints a series of ionized edges in the transmitted spectrum, leading to the observed complex low-energy absorption and a deep iron K edge at ~8 keV (Kallman & Krolik

★ Present address: Department of Physics, University of Durham, South Road, Durham DH1 3LE.

Downloaded from https://academic.oup.com/mnras/article/275/2/417/993736 by guest on 21 August 2022

© Royal Astronomical Society • Provided by the NASA Astrophysics Data System

1995MNRAS.275..417D

1987; Pounds et al. 1990; Nandra & Pounds 1992; Nandra & Pounds 1994, hereafter NP94). The iron line and high-energy excess are both consistent with an origin in X-ray illuminated cold material subtending a substantial solid angle $\sim 2\pi$ to the X-ray source (Piro, Yamauchi & Matsuoka 1990; Pounds et al. 1990; Fiore et al. 1992; NP94). Only ~ 10 per cent of the illuminating photons are reflected from this material, with the remainder being thermalized, to emerge at the local blackbody temperature. This broad, multitemperature spectrum, is similar to that predicted from a viscous accretion disc (Clavel et al. 1992; Matt, Fabian & Ross 1993), so that reprocessed hard X-ray flux can then explain both the variability and the spectrum of the UV/optical emission. Direct support for this reprocessing model was found from another monitoring campaign on NGC 5548 which showed correlated hard X-ray and UV flux variability (Clavel et al. 1992), although this correlation did break down with the addition of archival data, suggesting that both reprocessing and intrinsic disc emission may be important when the source is bright (Clavel et al. 1992). The detection of correlated, rapid UV–optical variability in other AGN (Clavel et al. 1990; Courvoisier & Clavel 1991; Reichert et al. 1994), together with the observation of the X-ray reflection signature in many Seyfert 1s, has led to the widespread acceptance of hard X-ray reprocessing as the origin for the 'big blue bump' in low-luminosity AGN.

The stability of the observed hard X-ray spectral index in Seyfert 1s can also be explained in such reprocessing models. The radiating electrons produce the hard X-ray flux, half of which is reprocessed in the disc into soft X-ray/UV emission, which in turn provides the seed photons for Compton cooling of the hot electrons (Haardt & Maraschi 1993, hereafter HM93). With complete feedback (e.g., a plane-parallel disc–corona geometry), where all of the reprocessed photons are available to cool the electrons, the approximate equipartition between the soft and hard luminosities then leads naturally to $\alpha \sim 0.9$–1 (HM93), as observed (Pounds et al. 1990; NP94). Such models have also been successful in fitting the X-ray data above 100 keV (Zdziarski et al. 1994, 1995), as well as the spectra of several Galactic black hole candidates (Haardt et al. 1993; Ueda, Ebisawa & Done 1994).

Here we describe the results of a recent *ROSAT* monitoring campaign on NGC 5548 in 1992 late December–1993 January. Since the *ROSAT* bandpass from 0.1 to 2 keV normally contains significant fluxes from both the power-law continuum, and soft excess emission from the disc, the variability of the two components can be studied simultaneously to constrain the reprocessing models described above. The warm absorber is also often prominent in this bandpass, with the ionized oxygen K edge and the L edges from iron being the main features (Nandra & Pounds 1992; Nandra et al. 1993). Any observed changes in the ionization state of the absorbing material can be used to constrain the density and geometry of this component, and, for example, see if it has a scale size consistent with the scattering region required in the Seyfert unification schemes.

2 OBSERVATIONS

ROSAT made 25 observations of NGC 5548 at approximately daily intervals during the month-long monitoring campaign. In addition, there was a single, long observation of NGC 5548 (92b) just as the monitoring campaign started, and two further observations, one early in 1992 (92a), and one in mid-1990. All these data were extracted from the images, background-subtracted, and rebinned into the SASS energy channels. Details of all the observations are given in Table 1.

Fig. 1 shows the total (0.1–2.5 keV: SASS channels 9–40), hard (1–2.5 keV: SASS channels 26–40) and soft (0.1–0.4 keV: SASS channels 9–16) X-ray count rates, together with their hardness ratio. The 92b data were taken on the same day as the first monitoring data set (01), and the two data sets are consistent in both intensity and hardness ratio. Thus spectra 92b and 01 were co-added to form a ~ 10-ks spectrum, hereafter called 01b, which is slightly higher in intensity, and somewhat softer than the 92a data taken nearly a year earlier.

The gain changes of the *ROSAT* detector between 1990 and 1992 mean that the channel ranges for the 1990 spectrum are not compatible with the rest of the data. However, on current understanding, this effect is small and the 1990 data can be plotted on the same scale as the later observations. It is clearly a much harder and fainter spectrum (Fig. 1).

During the monitoring campaign, there is clear evidence that both hard and soft energy bands are highly variable, but with rather different behaviour. The soft light curve is dominated by a factor 3 'flare' centred around the highest total flux states (day 10), whereas this feature is largely absent from the hard light curve. This differential variability leads to a strong change in hardness ratio during the flare, with a marked softening in the highest flux states. This behaviour might be expected from a source in which the hard power-law flux increases, causing further ionization of the warm absorber and hence a decrease in soft X-ray opacity. However, Fig. 2 shows a ratio of counts of the softest spectrum, 06, with that of the spectrum before the start of the flare, 01b. There is no apparent variability above 1 keV, where the spectrum should be dominated by the power-law flux; thus it seems that the hard power law is *not* the dominant driver of the variability. The major spectral change is a sharp rise in flux below 0.5 keV, much too low an energy to represent changes in the opacity of an ionized absorber, as this is dominated by the oxygen edge at ~ 0.7–0.8 keV. The strong softening seen in the raw data must then represent a separate soft X-ray excess component, which can vary independently of the hard X-ray flux. This is entirely contrary to the predictions of a pure reprocessing origin for the spectral variability. The power law has not changed in intensity, so it cannot drive changes in the reprocessed flux or ionization parameter, and yet the soft emission has increased markedly.

Thus, independent of detailed spectral fitting, we can already see that the reprocessing models described in the introduction are clearly inadequate to describe the variability seen during the monitoring campaign.

3 SPECTRAL FITTING

Some of the spectra still had less than 20 counts per SASS bin. These were further binned to ensure that χ^2 fitting was appropriate (more than 20 counts in each channel), which affected at most the last two energy bins. There is still some

Downloaded from https://academic.oup.com/mnras/article/275/2/417/993736 by guest on 21 August 2022

© Royal Astronomical Society • Provided by the NASA Astrophysics Data System

1995MNRAS.275..417D

Table 1. Observation log for NGC 5548.

ROR	Start Date	Start Time (UT)	End Time (UT)	Exposure (sec)	Name	
150071p	16 Jun 1990	23:29:07	132:43:52	17917	90	
700536p	17 Jan 1992	23:18:50	153:04:56	11136	92a	
701238p	24 Dec 1992	23:27:33	24:05:42	1676	01	coadded to
700536p	25 Dec 1992	09:09:58	16:05:12	8128	92b	form 01b
701239p	26 Dec 1992	00:56:36	01:37:13	1765	02	
701241p	28 Dec 1992	03:55:19	04:39:10	2006	03	
701242p	29 Dec 1992	05:27:49	06:11:19	1942	04	
701243p	30 Dec 1992	03:52:16	04:26:26	1984	05	
701244p	31 Dec 1992	02:02:58	02:43:39	1976	06	
701246p	02 Jan 1993	05:07:12	05:49:13	2013	07	
701247p	03 Jan 1993	05:01:20	05:48:25	2315	08	
701248p	04 Jan 1993	03:20:45	03:58:23	1904	09	
701249p	05 Jan 1993	03:11:18	03:52:40	1924	10	
701270p	06 Jan 1993	04:45:26	05:32:12	2364	11	
701271p	06 Jan 1993	09:32:12	32:38:12	6473	12	
701273p	09 Jan 1993	04:36:25	05:15:20	2258	13	
701275p	11 Jan 1993	14:27:48	14:38:34	546	14	
701276p	12 Jan 1993	14:15:57	14:33:23	595	15	
701277p	13 Jan 1993	14:22:47	14:28:17	221	16	
701279p	15 Jan 1993	14:01:23	14:17:30	649	17	
701280p	16 Jan 1993	13:52:29	15:48:17	1291	18	
701281p	17 Jan 1993	12:15:32	12:31:52	832	19	
701282p	18 Jan 1993	12:04:34	12:26:42	979	20	
701288p	24 Jan 1993	14:40:01	15:03:07	697	21	
701290p	26 Jan 1993	09:36:35	10:09:56	1504	22	
701291p	27 Jan 1993	09:31:51	10:04:20	1556	23	
701292p	28 Jan 1993	09:29:50	09:57:41	1476	24	
701293p	29 Jan 1993	07:45:13	08:18:52	1803	25	

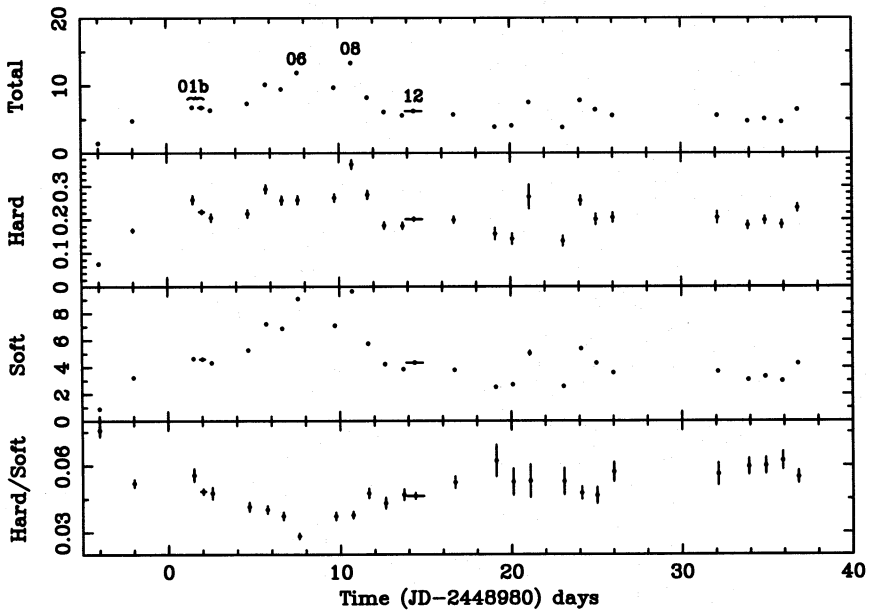

Figure 1. From top to bottom this shows the total (0.1–2.5 keV), hard (1–2.5 keV) and soft (0.1–0.4 keV) *ROSAT* count rates, together with the hardness ratio. Names of individual spectra used in the text are indicated.

considerable uncertainty in the PSPC response matrix, with DRM06 recommended for data taken in AO1, and DRM36 for later observations. The differences between these two matrices is also a crude guide to the size of remaining systematic errors (Osborne 1993). A ratio of the two matrix effective areas gives a difference of ~2 per cent below 2 keV (except around the carbon edge), so we added this amount of systematic error to all the data sets. However, the true calibration errors are certainly more complex than this procedure implies, and may also be considerably larger (Osborne 1993; Turner 1993; Fiore et al. 1994).

The poor resolution of the *ROSAT* PSPC means that a

Downloaded from https://academic.oup.com/mnras/article/275/2/417/993736 by guest on 21 August 2022

© Royal Astronomical Society • Provided by the NASA Astrophysics Data System

1995MNRAS.275..417D

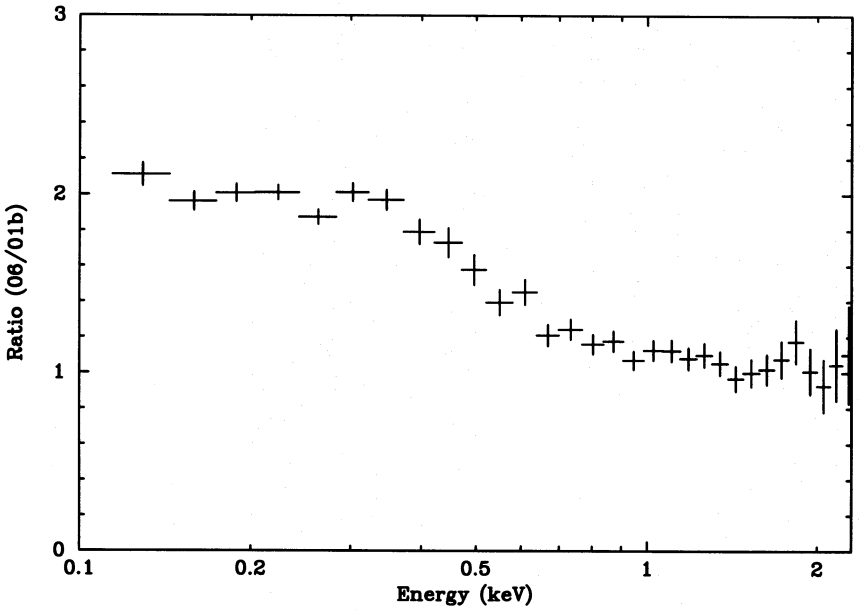

Figure 2. The ratio of *ROSAT* spectra from 01b and 06. Clearly, the spectral variability primarily affects the spectrum below 0.4 keV.

Table 2. Spectral fits to 01b.

	α	$N_{pl}{}^a$	$kT_{th}{}^b$	$N_{th}{}^c$	ξ^d	$N_H{}^e$	χ^2_ν/dof
A	1.36 ± 0.01	1.69 ± 0.02					2.87/30
B	1.07 ± 0.07	1.60 ± 0.03	75 ± 3	3.3 ± 0.7			1.19/28
C	$1.29^{+0.16}_{-0.10}$	$2.10^{+0.07}_{-0.19}$	$127^{+73}_{-41}{}^f$	$0.88^{+0.91}_{-0.68}$	18^{+60}_{-12}	$0.41^{+0.58}_{-0.20}$	0.40/26
D	$0.97^{+0.43}_{-0.15}$	$2.09^{+0.15}_{-0.57}$	$17, 77^g$	$29, 2.6^g$	430^{+600}_{-427}	$2.9^{+10.0}_{-2.45}$	0.40/24
E	0.67 ± 0.20	1.32 ± 0.14	245 ± 23	151 ± 12			0.70/28
F	$1.20^{+1.60}_{-0.28}$	$1.94^{+0.09}_{-1.87}$	399^{+748}_{-146}	356^{+688}_{-331}	17^{+370}_{-10}	$0.46^{+3.10}_{-0.23}$	0.41/26

[a]Normalization $\times 10^{-2}$ photon cm^{-2} s^{-1} at 1 keV; [b]Thermal temperature in eV; [c]Normalization of thermal component $\times 10^{-4}$; [d]Ionization state of the warm absorber; [e]Column density of the warm absorber $\times 10^{22}$ cm^{-2}; [f]The blackbody temperature was constrained to be less than 200 eV; [g]Error ranges are not given, as the component is poorly constrained.

unique deconvolution is not possible, especially where multiple components are expected to contribute to the spectrum. Prior knowledge of some spectral parameters is extremely helpful in disentangling the *ROSAT* data, so we first review the *Ginga* results in the 2–20 keV band.

3.1 The *Ginga* data

The multiple *Ginga* data sets for NGC 5548 have been analysed in Nandra et al. (1991) and NP94. The fits where both ionized absorption and the reflection model proposed by George & Fabian (1991) were included gave an average spectral index of $\alpha = 0.85 \pm 0.05$ (NP94). This reflection model includes the self-consistent line emission, assuming solar abundances. Decoupling the line emission from the reflection continuum, which allows for differences in abundance and/or uncertainties in the atomic data (e.g. Zycki & Czerny 1994), gives $\alpha = 0.91 \pm 0.07$ (see Done et al. 1994 for details of the fit), where the error range, here and elsewhere unless stated, is 90 per cent confidence for one interesting parameter, i.e. $\Delta\chi^2 = 2.7$.

3.2 The first monitoring data set

With this 'prior knowledge' of the intrinsic spectral index of the power-law component in NGC 5548 we can now turn to the *ROSAT* data. The co-added data from 1992 December 25 (01b) has the longest exposure of the monitoring campaign, ~10 ks, so the properties of this spectrum are discussed first. Details of all the spectral fits in this section are given in Table 2. As considerable uncertainties remain in the determination of the *ROSAT* PSPC response, these spectral results should not be overinterpreted, but rather seen as representative of the current matrix.

With the line-of-sight column density fixed at the Galactic value of $N_H = 1.65 \times 10^{20}$ cm^{-2}, where N_H is equivalent column of hydrogen atoms, a simple power law was an unacceptable description of the data, with $\chi^2_\nu = 2.87/30$ (model A). Also, the derived spectral index is $\alpha = 1.36 \pm 0.01$, much steeper than the *Ginga* power law as discussed above. With the spectral index fixed at $\alpha = 0.9$, the points above 2 keV, which are least affected by any soft excess or warm absorber, give an extrapolated 2–10 keV flux of 4.5×10^{-11} erg cm^{-1}

Downloaded from https://academic.oup.com/mnras/article/275/2/417/993736 by guest on 21 August 2022

© Royal Astronomical Society • Provided by the NASA Astrophysics Data System

1995MNRAS.275..417D

s^{-1}, corresponding to the highest intensity *Ginga* spectrum (NP94). Thus even before the large-amplitude flare in the monitoring campaign the source was close to its recorded maximum (Nandra et al. 1991).

The addition of a blackbody soft excess gave a much improved fit, with $\chi^2_\nu = 1.19/28$, and a flatter power-law spectral index of $\alpha = 1.07 \pm 0.07$, and $kT = 75$ eV (model B). The addition of a warm absorber led to a further significant improvement ($\gg 99$ per cent confidence on a two-parameter F test), with $\chi^2_\nu = 0.40/26$ (model C), but the derived spectral index steepened to $\alpha \sim 1.3$. We note that a steep index may be indicative of a further soft excess component, and indeed, if this is associated with the accretion disc, then the range of emission radii predicts a multitemperature spectrum, i.e. broader than a single blackbody form. There is considerable uncertainty over the precise shape of this disc spectrum, but most simple models are a radial sum of quasi-blackbody spectra at the local temperature (see, e.g., Frank, King & Raine 1992). We use two blackbodies to approximate the disc spectrum in the *ROSAT* band, which gives an excellent fit to the data, with $\chi^2_\nu = 0.40/24$ (model D). While this additional blackbody component is not required statistically by the data, it led to an appreciable flattening of the intrinsic spectrum with respect to that derived from a single blackbody and warm absorber, so that the power law is now consistent with the *Ginga* results.

An alternative origin for a broad soft X-ray excess is bremsstrahlung emission. This has been proposed as a mechanism to produce the whole optical/UV blue bump in AGN (Barvainis 1993, and references therein), and has the advantage that it explains the broad-band nature of the spectrum and the correlated optical/UV variability seen in these objects. Multiple emitting clouds which are effectively optically thin at UV energies are proposed to circumvent the limits on variability from a single region, and these can be either optically thin or thick to electron scattering. In the latter case, they can also intercept the incident X-ray radiation, and reprocess it to form both the reflection spectrum and iron Kα line, as well as the optically thin UV continuum. However, the soft X-ray spectrum is then quasi-blackbody in shape (e.g. Rybicki & Lightman 1979), and so the spectrum differs little from the modelling described above. In the former case, where the clouds are optically thin to electron scattering, the emission spectrum is a bremsstrahlung continuum across the whole UV/soft X-ray band, but probably with little associated line emission because of strong overionization of the clouds from coronal plasma models due to to photoionization. However, for this description the clouds do not absorb a large fraction of the incident X-ray energy, and so their source of heating remains extremely *ad hoc*. With a bremsstrahlung description of the soft X-ray excess (model E) the derived power-law spectrum is *flat* because of the slower fall-off of the bremsstrahlung continuum at high energies compared to that of a blackbody. However, the model shows significant improvement with the addition of a warm absorber (model F), with $\Delta\chi^2 = 9$, and the derived spectrum is then consistent with the *Ginga* power-law index range.

A completely different, non-emission, origin for a broad soft excess is reflection from partially ionized material. The surface of the accretion disc is exposed to an intense illuminating X-ray flux, so some ionization of the surface layers is likely. This changes the shape of the reflection spectrum from that of neutral material as the reduced photoelectric opacity at low energies in ionized material leads to enhanced reflection (Lightman & White 1988; Netzer 1993; Ross & Fabian 1993; Zycki & Czerny 1994). A strong oxygen K edge in the reflected spectrum can lead to the situation where there is a considerable amount of reflection below 0.8 keV, but little above, mimicking the effect of a broad soft X-ray *emission* component (Czerny & Zycki 1994). Firm limits on the amount of ionization of the reflection spectrum can be obtained from the *Ginga* hard X-ray spectra. Fitting a power-law, ionized reflector (one-zone calculation of the ionization balance as implemented in the pliref model in the XSPEC spectral fitting package; Lightman & White 1988; Done et al. 1992) and ionized absorber to the brightest *Ginga* data set, that of 1989 July 13 (NP94), gives a solution in which the ionization state of the reflector, $\xi_{\rm ref} \leq 120$ at 90 per cent confidence ($\Delta\chi^2 = 2.7$). This low limit on the ionization parameter means that substantial amounts of ionized reflection contributing to the soft X-ray spectrum can be ruled out at high confidence in this object.

All the acceptable models for the *ROSAT* data in Table 2 require the partially ionized absorber (C, D and F). Of these, only D and F (double blackbody and bremsstrahlung) give spectral indices that overlap with those derived from the 2–20 keV data (Table 2), while the other model gives a substantially deeper power-law index than is seen at higher energies. While mechanisms exist for producing a *flatter* power-law slope at low energies (Haardt & Maraschi 1991; HM93), there is no physical reason to expect a steeper spectrum, although it could be symptomatic of miscalibration of the instrument response. Since we have no better information on the response, we chose a broad emission component (double blackbody or bremsstrahlung) and warm absorber to model the deviations from a power-law spectrum in the monitoring campaign data.

3.3 The soft spectra

The monitoring campaign data show clear spectral variability, as well as changes in flux level (see Figs 1 and 2). In a reprocessing model for the soft excess, the soft flux should map any changes in the hard power-law intensity. Any temperature variations should be small, since $L_{\rm soft} \propto T^4$. A factor 2 intensity variability should lead to a change in temperature of ≤ 20 per cent, which can be neglected. In our two-temperature blackbody description of the soft X-ray excess, this is equivalent to a model in which the temperatures and ratio of normalizations of the two soft components are constant, as is the ratio of normalizations of the blackbodies to that of the power law. We incorporated such a model into the XSPEC spectral fitting package, and used this, together with the warm absorber, to fit the first and softest spectra simultaneously (01b and 06). Only the normalization of the power-law components and the ionization states were allowed to vary independently between the two data sets, and the resulting model is an acceptable fit to the spectra (model A), with $\chi^2_\nu = 0.85/54$, for $\alpha \sim 1$ (Table 3). However, the derived power-law intensity is a factor 2 brighter in 06 than in 01b, but with an ionization parameter 10 times smaller. Also, an extremely significant decrease in χ^2_ν to 0.45/53, is obtained by allowing the relative normalization of the soft excess with

Downloaded from https://academic.oup.com/mnras/article/275/2/417/993736 by guest on 21 August 2022

© Royal Astronomical Society • Provided by the NASA Astrophysics Data System

1995MNRAS.275..417D

Table 3. Spectral fit to 01b and 06.

		$N_{pl}{}^a$	$N_{th}/N_{pl}{}^b$	ξ^c	χ^2/dof
A	01b	$1.72^{+0.32}_{-0.18}$	1.67 ± 0.7	2500 ($\geq$ 880)	0.85/54
	06	$3.42^{+0.7}_{-0.4}$		220 ± 40	
B	01b	1.90 ± 0.18	$1.4^{+0.55}_{-0.80}$	315^{+2700}_{-200}	0.45/53
	06	$1.63^{+0.14}_{-0.08}$	$6.3^{+0.8}_{-1.3}$	10^4 ($\geq$ 100)	

[a]Normalization $\times 10^{-2}$ photon cm^{-2} s^{-1} at 1 keV; [b]Ratio of the highest temperature blackbody component normalization to that of the power law $\times 10^{-2}$; [c]Ionization state of the warm absorber.

respect to the power law to be variable (model B). The unfolded spectra using this best-fitting model (Fig. 3) show that the power law is almost identical in intensity in the two data sets, while the soft excess has dramatically increased, which is in marked conflict with the predictions of reprocessing models and confirms the preliminary conclusions drawn from the ratio of the two spectra given in Section 2. Neither the spectral index nor the ratio of the two blackbody components (i.e. the shape of the soft X-ray excess) shows any significant further decrease in χ^2 if they are allowed to vary between the two data sets.

A similar result is derived for the bremsstrahlung description of the broad soft X-ray excess component, with χ^2_ν decreasing from 0.98/56 to 0.63/55 when the ratio of the bremsstrahlung to the power law is allowed to vary between the two data sets. Thus the data are consistent with a model in which the soft excess and power law are constant in shape but whose relative contribution to the spectrum can vary substantially.

In order to check this conclusion, a more general model was constructed in which the ratio of the total luminosity in the two blackbody components to that of the power law is a free parameter, without constraining the shape of the soft excess to be the same in each spectrum. With this model an excellent fit can be obtained if the lower temperature blackbody component is very strong in the 01b data set, and at a low temperature. This large-luminosity component is mostly unobservable by *ROSAT*, and the hidden flux can then be transferred to the higher temperature component (which dominates in the *ROSAT* energy range) in the 06 spectrum, as required by the data. While such a model is consistent energetically with a reprocessing scenario, the derived hard X-ray power law is again almost identical between the two data sets, so conflicting with reprocessing models since we require a large shift in the effective temperature of the soft excess without any driving change in the hard X-ray power law. Thus it seems that reprocessing models alone cannot adequately describe the observed spectral variability in these data.

3.4 The total data set

The 25 monitoring data set spectra (01b–25) were then fitted simultaneously to determine the time variability of the power law, soft excess and warm absorber. The power-law index, warm column density, and shape of the soft excess were assumed to be constant, while the ionization state, normalization of the soft excess with respect to the power law, and the power-law intensity were free to vary independently. This gave an excellent fit ($\chi^2_\nu = 0.92/692$) to the data, with $\alpha = 0.94$ and $N_{\rm H} = 2.4 \times 10^{22}$ cm^{-2}. The double blackbody model for the soft excess is required at high significance: a single blackbody gave a $\Delta\chi^2 \sim 60$ for the removal of two free parameters (the soft blackbody temperature and its normalization ratio with respect to the higher temperature blackbody), confirming that a broad soft excess is required irrespective of any constraint that the spectral slope be consistent with the *Ginga* values. The bremsstrahlung model is a worse description of the soft excess, giving an increase in χ^2

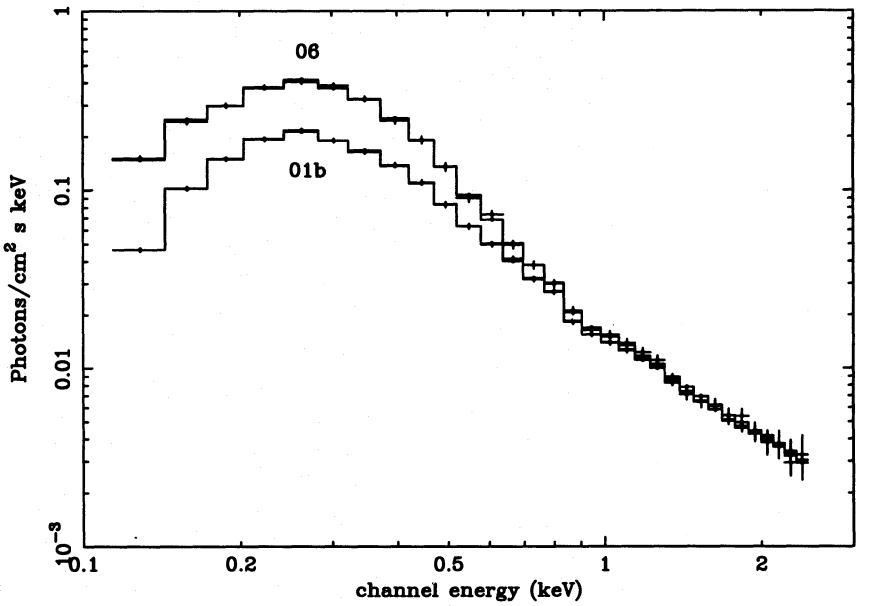

Figure 3. The unfolded spectrum for simultaneous fitting of 01b and 06 with a model in which the ratio of the broad soft excess component to the power-law flux is allowed to vary independently between the two data sets.

Downloaded from https://academic.oup.com/mnras/article/275/2/417/993736 by guest on 21 August 2022

© Royal Astronomical Society • Provided by the NASA Astrophysics Data System

1995MNRAS.275..417D

of ~28, so in all that follows we use the double blackbody shape.

Error ranges are rather hard to assign for such complex models, where many of the parameters are highly correlated. However, in fitting 25 spectra simultaneously, the parameters that are tied across the total data set are not greatly affected by changing the normalizations in any single spectrum. Thus approximate error ranges on these parameters can be found by fitting each single spectrum with the double blackbody, power-law and ionized absorption model, freezing the tied parameters at the best-fitting values derived from the simultaneous spectral analysis. There are then three free parameters which are all correlated with each other, so $\Delta\chi^2 = 3.53$ is used to derive the 1σ error bars. This single spectral fitting was redone with a double blackbody model in which the hotter blackbody norm was the fitted parameter, rather than its ratio to the power-law flux. This enabled error ranges on the blackbody flux to be derived from a single parameter. The light curves from these fits are shown in Fig. 4.

The blackbody flux varies by a factor of ~10, while the power-law flux varies only by a factor of 2–3. Consequently, there is large variability in their ratio. Reprocessing models make the strong prediction that the soft-component variations should be driven by the power-law variability. This is clearly not the case in the first part of these data where there is a strong softening event taking place over an 8-d period. The plot also shows the large errors on the derived ionization parameter, which are consistent with it either being constant or proportional to the flux. Spectrum 16 (day 21) has a rather smaller ionization parameter than would be expected for its high power-law flux, but the error bars are rather large and the derived intensity could be misleading as the 200-s exposure is less than a single 'wobble' period of the satellite.

The simultaneous spectral fitting also confirms that the data cannot reliably constrain the ionization parameter in each individual spectrum. A single ionization parameter tied between all the spectra is not a significantly worse fit to all the data, with $\chi^2_\nu = 0.93/716$ for $\alpha = 0.91$, $N_H = 5.8 \times 10^{22}$ cm^{-2} and $\xi = 710$. Similarly, setting the ionization parameter to scale with the total flux also gives a good fit, with $\chi^2 = 0.92/716$, for $\alpha = 0.90$, $N_H = 4.8 \times 10^{22}$ cm^{-2} and $\xi_{01b} = 723$. However, large changes in ionization parameter are clearly not expected throughout the data, as there are several sections of the light curve where there is no dramatic variability (see Fig. 4). Also, there are several spectra with short exposure times, which are much less likely to be able to constrain the ionization parameter. The longest exposure monitoring spectrum, 12, is a factor of 2 dimmer than the brightest spectrum, 08, so a comparison of these two spectra is the most promising place to look for a decrease in ionization. Fixing the ionization state to be equal in these two spectra, while all the other ionization parameters are allowed to be free, leads to a change in χ^2 of 8, significant at ≥ 99 per cent confidence on a one-parameter F test.

Confidence contours for the ionization parameter change are extremely difficult to produce from the simultaneous spectral fits, so again we use the fact that the parameters tied across all the data sets are not greatly affected by any changes in the fit of one or two individual spectra. Thus these parameters can be frozen, and just the two spectra for which the ionization state is to be compared are fitted simultaneously. The change in ionization between 08 and 12 is significant, and consistent with being proportional to the change in flux, as shown by the confidence contours in Fig. 5(a). There is a significant, but subtle, change in the spectrum of NGC 5548 between these two data sets, and the short time-scales involved make it unlikely that this is due to the detector gain drift. It may, however, be caused by changes in the shape of the soft excess rather than by changes in the ionization parameter.

Similarly, the most promising place to look for an increase in ionization is between 01b and 08. Here, however, the change in flux is slightly less, and Fig. 5(b) shows that while

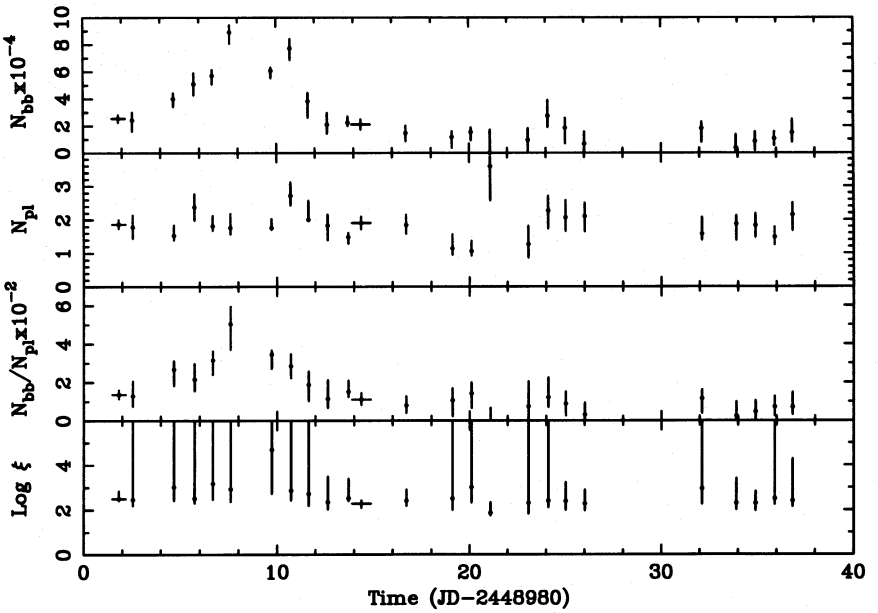

Figure 4. The derived light curve from the monitoring data. From top to bottom these are the normalization of the hottest blackbody, the normalization of the hard power law, their ratio and the (poorly constrained) ionization parameter.

Downloaded from https://academic.oup.com/mnras/article/275/2/417/993736 by guest on 21 August 2022

© Royal Astronomical Society • Provided by the NASA Astrophysics Data System

1995MNRAS.275..417D

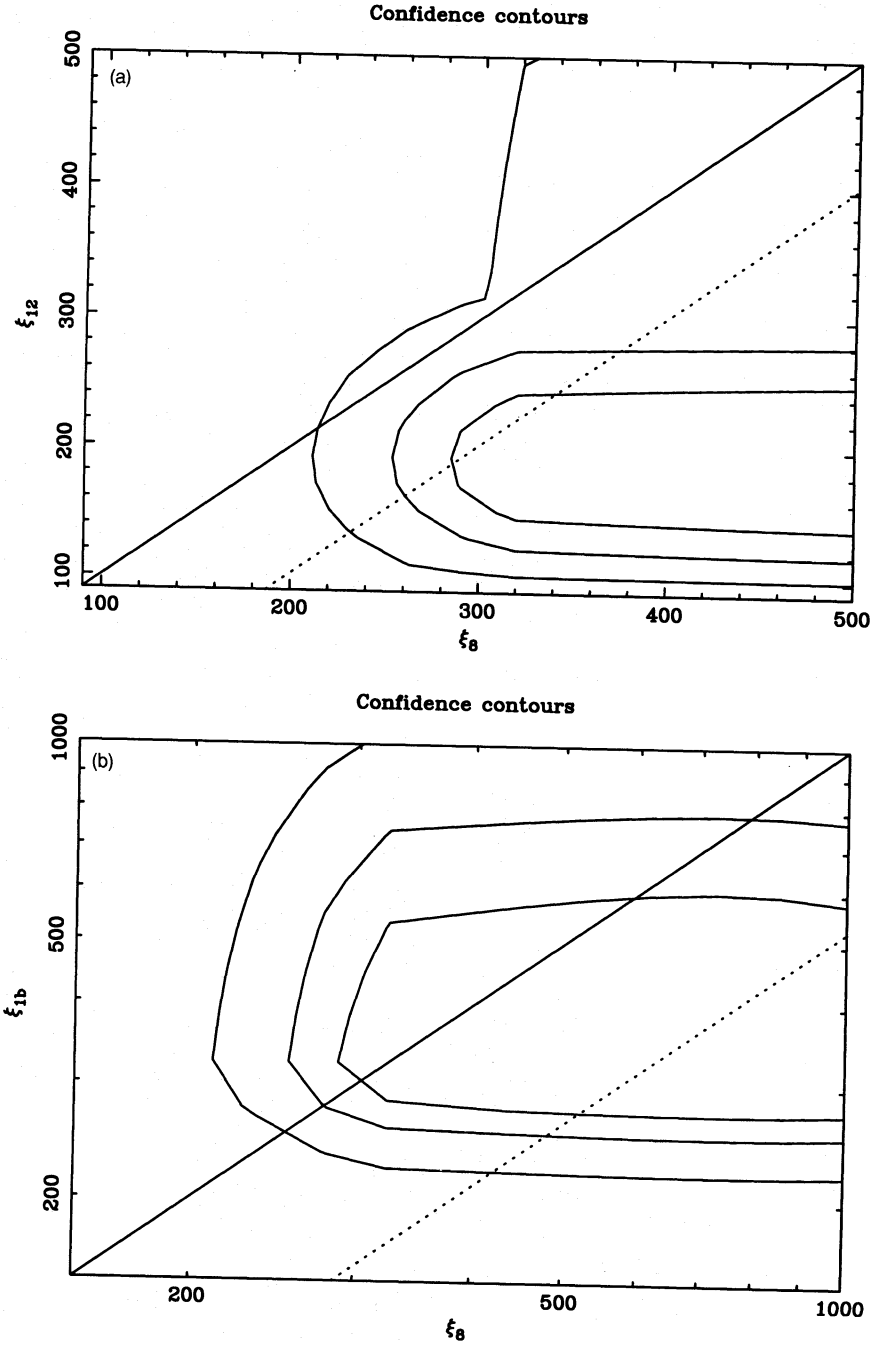

Figure 5. (a) Confidence contours for the ionization parameters in spectra 08 and 12, showing a significant decrease between the two data sets. The solid line indicates a constant ionization parameter, while the dotted line assumes that the ionization is proportional to flux. (b) As for (a), for spectra 08 and 01b. These data are consistent with an increase proportional to flux, but this is not required.

the data are consistent with a change in ionization proportional to flux, this is not required by the data.

The three parameters describing the soft excess shape are the two blackbody temperatures of 24^{+8}_{-9} and 80^{+7}_{-5} eV, respectively, and their ratio of normalizations, $2.4^{+17.3}_{-0.6}$. As all three parameters are strongly correlated, the errors quoted are for 68 per cent confidence with three interesting parameters, i.e. $\Delta\chi^2 = 3.53$.

The column density is not well constrained by the data, with a minimum in χ^2 space that is not smooth, as shown by Fig. 6(a). The derived best-fitting spectral index for each column density is shown in Fig. 6(b). The two parameters are correlated over the range $(0.7\text{–}7)\times 10^{22}$ cm^{-2} in the sense of higher columns preferring a flatter intrinsic power law. However, for extremely high columns, the derived spectral index rises slowly again since the complexity of spectrum of the warm absorber decreases at high ionization parameters (i.e. high columns), where it is well represented by a single oxygen edge. Superimposed on Fig. 6(a) is the column derived from the models where the ionization parameter is constrained to be either constant (dashed line), or varying proportionately with flux (dotted line). The column is much better deter-

Downloaded from https://academic.oup.com/mnras/article/275/2/417/993736 by guest on 21 August 2022

© Royal Astronomical Society • Provided by the NASA Astrophysics Data System

1995MNRAS.275..417D

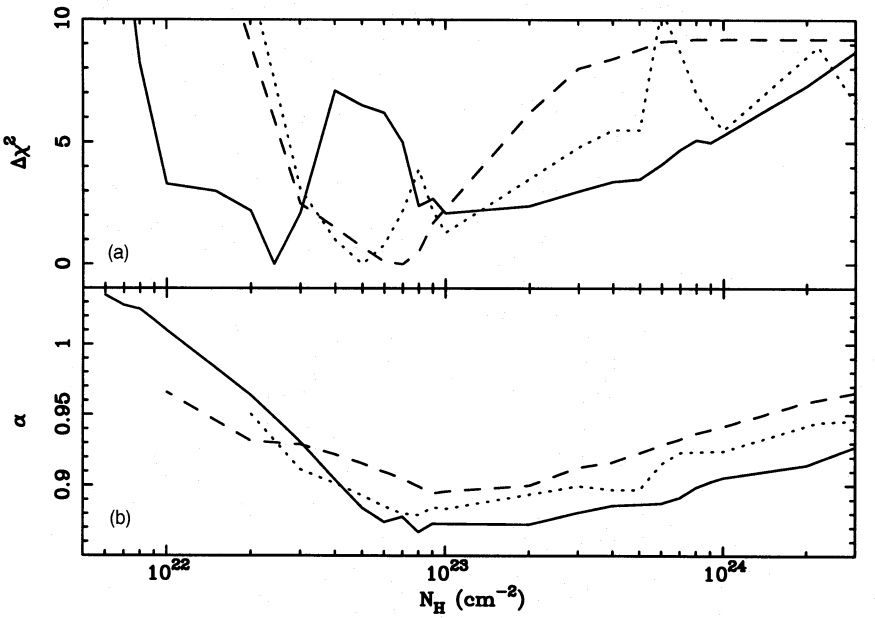

Figure 6. The solid, dotted and dashed lines refer to models in which the ionization parameter is free, proportional to flux, and constant, respectively. The change in χ^2 with varying column density of the warm absorber is shown in the upper panel, while the best-fitting spectral index for the resulting fit is shown in the lower panel.

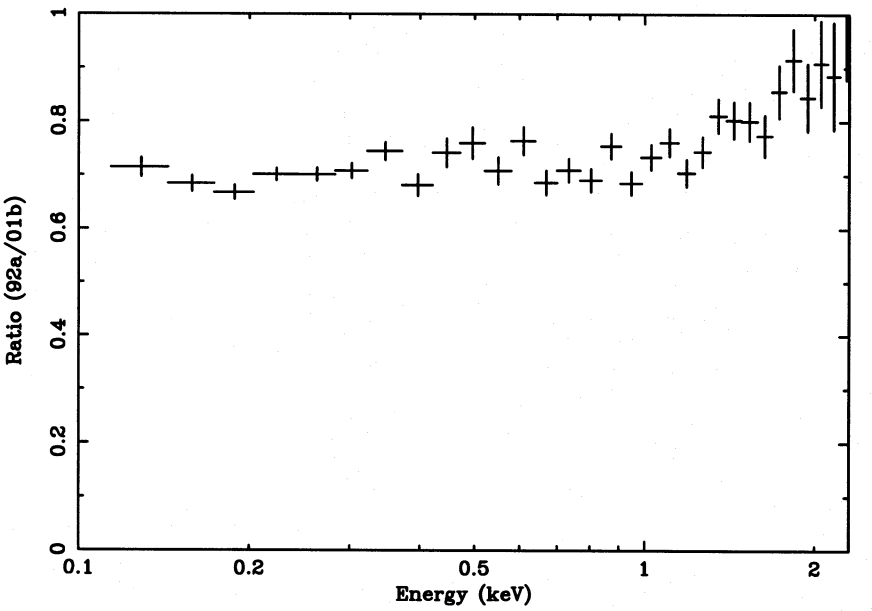

Figure 7. The ratio of *ROSAT* spectra from 92a and 01b. The 92a data set is similar in shape to 01b, but lower in intensity below 1 keV as the ratio is constant. However, the ratio rises steeply between 1 and 2 keV, indicating that there are subtle differences in the shape of the hard spectrum in the two data sets.

mined in these models, as there are 24 fewer free parameters. The correspondingly derived spectral index is shown in Fig. 6(b).

In summary, the monitoring data thus show strong differential variability of the soft excess and power-law components, with some evidence for further spectral variability from changes in the ionization parameter. The power-law spectral index is consistent with remaining constant throughout these changes, with $0.83 \leq \alpha \leq 1.02$ within $\Delta\chi^2 = 10$ of the best-fitting values.

3.5 The previous *ROSAT* spectra

The spectrum taken in 1992 January (92a) may not be directly comparable with the monitoring data due to uncalibrated gain drift over this period (Turner 1993). However, below 1 keV these gain problems seem small, with a change of less than 10 per cent between data taken in 1992 and 1993 (Turner 1993). A ratio of the 92a data to those of spectrum 01b (Fig. 7) is flat to within 10 per cent below 1 keV, showing that the soft spectral shape is consistent with that

Downloaded from https://academic.oup.com/mnras/article/275/2/417/993736 by guest on 21 August 2022

© Royal Astronomical Society • Provided by the NASA Astrophysics Data System

1995MNRAS.275..417D

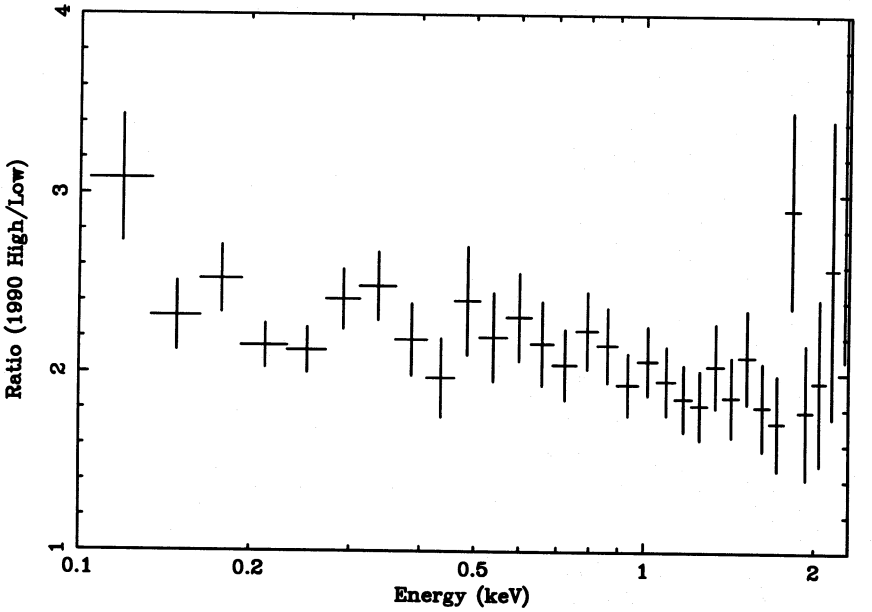

Figure 8. The ratio of high- to low-intensity states in the 1990 *ROSAT* data sets. Clearly, the main change is in the power-law intensity.

derived from the monitoring data. At higher energies the 92a data have increasingly more hard photons with respect to its soft flux than 01b. This is a monotonic rise of 20–30 per cent, rather larger in magnitude and different in shape to the changes induced by the response matrix gain drift (Turner 1993) but, given the calibration uncertainties, we cannot reliably interpret these as a real change in the hard spectrum (power-law index or warm absorber column density) of the source.

The 1990 data definitely cannot be directly compared to the 1992–1993 spectra, as these data were taken before the gain change on 1991 October 14, and in a different detector (PSPC-C rather than PSPC-B). Preliminary studies of the calibration source N132D indicate that there are *substantial* time-dependent gain variations between 1990 and 1993 which are not removed by the current gain correction procedure (Turner 1993), so until these effects are understood we caution against detailed interpretation of the apparent variability in spectral shape between data taken before and after the gain/detector change. However, the 1990 data on NGC 5548 show substantial variability during the observation (Nandra et al. 1993), so *relative* spectral changes within these data should be secure.

We use the same three intensity state spectra as given by Nandra et al. (1993). A ratio of the high- and low-state data sets is given in Fig. 8, clearly showing that the main difference is a change in the underlying power-law intensity. There is slightly more difference at low energies than at high, with the transition being at ~ 0.8 keV. Fitting a constant to the spectral ratio below 0.6 keV gave a mean value of $2.28^{+0.08}_{-0.10}$ as opposed to the 1–2 keV mean of $1.93^{+0.07}_{-0.12}$, so the 90 per cent error bars to not overlap. As the transition energy is close to the oxygen K edge, this may be related to a change in the ionization parameter between the two data sets, rather than to a change in the ratio of soft excess to the power-law flux. If so, the sense of the change is that there is *more* edge present in the high-state data, i.e. that it represents a lower ionization state. This is confirmed by simultaneous spectral fitting of the three 1990 data sets to a power law, soft excess and ionized absorber. With a single blackbody description of the soft excess, the soft component *is* consistent with maintaining a constant ratio to the power-law component throughout the 1990 data, but only if there is a significant decrease in the ionization parameter between the low- and high-state spectra, i.e. for an ionization that is anticorrelated with flux level. If the ionization parameter follows the flux, then the ratio of the soft component to power-law flux increases as the source brightens. With all of these descriptions, the power-law index is rather flat, with $\alpha \sim 0.58 \pm 0.06$, rather than the $\alpha \sim 0.9$ seen in the monitoring data. However, given the current uncertainties in the response matrix, this may not represent a real change in source spectrum.

Thus, while the variability of the 1990 data is consistent with that predicted by the reprocessing scenarios described in the introduction, a better calibration of these data is required to assess the applicability of current theoretical models.

4 DISCUSSION

The *ROSAT* X-ray monitoring campaign of NGC 5548 provides the best time series to date for examining the variability of the hard power law, soft excess and ionized absorber. The observations were taken while the source was at its maximum recorded brightness level, with an inferred unabsorbed 2–10 keV power-law flux of up to $\sim 7.6 \times 10^{-11}$ erg cm^{-2} s^{-1} (spectrum 08; cf. fig. 1 in Nandra et al. 1991). Assuming that this spectrum extends to ~ 300 keV (Zdziarski et al. 1994, 1995), the total hard X-ray luminosity is then $\sim 5.5 \times 10^{44}$ erg s^{-1}, for $H_0 = 50$ km s^{-1} Mpc^{-1}. For a likely black hole mass range of $10^{7\text{–}8}$ $M_\odot$ (Krolik et al. 1991), the system was accreting at ≥ 0.1 of its Eddington luminosity during the monitoring campaign.

The campaign also showed variability in the hard X-ray power-law intensity, with changes of a factor of 2 in 1 d, indicating a compactness $\ell = L/R \times \sigma_T/m_e c^3 \sim 7$, comparable

© Royal Astronomical Society • Provided by the NASA Astrophysics Data System

Downloaded from https://academic.oup.com/mnras/article/275/2/417/993736 by guest on 21 August 2022

1995MNRAS.275..417D

with previous estimates (e.g. Done & Fabian 1989). The soft X-ray spectrum below 0.5 keV is largely dominated by a soft excess component which varies independently of the hard X-ray flux, most noticeably in a soft X-ray flare lasting ~ 8 d, which has no hard X-ray counterpart. This behaviour is incompatible with the correlated variability predicted from simple accretion disc reprocessing models. This conclusion can be seen from simple ratios of the monitoring data sets, and so is independent of any modifications to the *ROSAT* response to account for the long time-scale changes in gain.

The decoupling of the soft emission from that of the hard X-rays can be explained most easily if there is a separate source of soft emission during the flare event. Given the unusually high luminosity of the source during the campaign, it is likely that the intrinsic emission from the accretion disc itself is not negligible. While the derived temperature of this emission is rather higher than would be expected from standard thin α-disc equations (~ 50 eV as opposed to the observed temperature of 80 eV; Shakura & Sunyaev 1973), the detailed shape of the spectrum may well change with newer assessments of the *ROSAT* response. Also, the thin disc approximation breaks down at accretion rates of ~ 0.1 times the Eddington luminosity (e.g. Frank et al. 1992), so if the temperature discrepancy remains, it can perhaps be explained by the disc puffing up in its inner regions, or by Compton scattering within the disc itself leading to enhanced higher temperature emission (Czerny & Elvis 1987; Ross, Fabian & Minishige 1992).

The alternative explanations for the origin of the soft excess considered in Section 3 are not very satisfactory. A reflection origin (Czerny & Zycki 1994) is incompatible with the limits on the ionization state set from *Ginga* data. Bremsstrahlung from multiple emission clouds that are effectively optically thin in the UV, but optically thick to electron scattering, can explain the broad-band nature of the spectrum and the rapid correlated optical/UV/X variability (Barvainis 1993). However, the soft excess is then still produced by reprocessing, and so should follow the hard X-ray flux. The soft flare would then have to be associated with a large increase in the number of these bremsstrahlung-emitting clouds, which seems extremely arbitrary.

Assuming that the soft emission is from the accretion disc, the flare time-scale of ~ 8 d could correspond to either the viscous time-scale for the response to a change in accretion rate (as the disc is no longer thin), or a thermal instability in the accretion disc. The former seems more likely, as there is a general trend for the hard and soft luminosities to go up and down together, although this trend is neither linear nor a strict correlation.

The observation of a strong increase in the soft component in NGC 5548 at high accretion rates may form a link between 'normal' Seyfert 1 AGN, where reprocessing is dominant, and the 'ultrasoft' AGN (Puchnarewicz et al. 1992; Boller et al. 1993; Brandt et al. 1994; Gondhalekar et al. 1994; Pounds 1995) which may be dominated by emission from the accretion disc. The 'ultrasoft' AGN would then be analogous to the high-state spectra from the Galactic black hole candidates, as suggested by Pounds (1995).

The warm absorber is clearly present in our data, but its ionization state is poorly constrained. However, there is evidence for flux-correlated variability in one of the two epochs during the monitoring campaign in which a changing ionization parameter could most easily have been seen, assuming that the soft excess shape remains constant. Since the brightest spectrum (08) has an ionization parameter of ~ 500 (cf. Figs 5a and b), oxygen, the dominant contributor to the spectrum, is mostly stripped, with only 10 per cent remaining as O VIII. The recombination time-scale is then $t_{\rm rec} = [n_{\rm e}\alpha({\rm O\,VIII})n({\rm O\,IX})/n({\rm O\,VIII})]^{-1}$ (Krolik & Kriss 1995), where $\alpha({\rm O\,VIII}) \sim 1.3 \times 10^{-11}$ cm^3 s^{-1} for a temperature of $\sim 10^5$ K is the radiative recombination rate for O XI to O VIII, and $n({\rm O\,IX})/n({\rm O\,VIII})$ are the relative populations of the two ions. This implies $n_{\rm e} \geq 5 \times 10^4$ cm^{-3} from the 2-d time difference between the two spectra. The thickness, R, of the absorber can in principle be estimated from the measured column. This is, however, poorly constrained by the data, with the range $2 \times 10^{22} \leq N_{\rm H} \leq 3 \times 10^{24}$ being within $\Delta\chi^2 = 10$ of the minimum for either a constant ionization parameter or one that varies proportionally to flux (Fig. 6a). Thus we can only give a weak upper limit of $R \leq 6 \times 10^{19}$ cm. If this material is in a thin shell, then the distance of the warm material from the central source can be obtained from the ionization parameter: $\xi = L/nr^2 \sim 500$, which implies that the material is $\leq 10^{18}$ cm from the X-ray source for an X-ray luminosity of $\sim 5 \times 10^{44}$ erg s^{-1}. This is clearly compatible with the estimates of the distance and physical state of the 'scattering region' required in Seyfert unification schemes (Krolik & Begelman 1986; Kallman & Krolik 1987).

However, the situation is almost certainly much more complex. The scattering region is associated with a geometrically thick, mildly supersonic outflowing wind (Krolik & Begelman 1986), in which the density and ionization state are a function of radial distance. Assuming a Mach number, M, of less than 10, we obtain a flow time-scale of $R/(Mc_{\rm s})$ s, where the sound speed, $c_{\rm s} \sim 10^4 T^{1/2} \sim 3 \times 10^6$ cm s^{-1} for a gas temperature of $\sim 10^5$ K. There is strong evidence from *ASCA* observations of MCG-6-30-15 (another Seyfert 1 with similar properties to NGC 5548; NP94) for a factor 2 change in the structure of the warm absorber in 3 weeks (Fabian et al. 1994), which then limits $r \sim R \leq 5 \times 10^{13}$ cm if this is a true change in column (but see Krolik & Kriss 1995). This is much smaller than the scattering region envisaged in the unification schemes, probably indicating that the wind is a highly structured and clumpy, rather than a smooth flow.

ACKNOWLEDGMENTS

CD, KN and ACF acknowledge support from a PPARC Advanced Fellowship, a PPARC Research Associateship, and the Royal Society, respectively.

REFERENCES

Antonucci R., 1993, ARA&A, 31, 473
Barvainis R., 1993, ApJ, 412, 513
Boller T., Trumper J., Molendi S., Fink H., Schaeidt S., Caulet A., Dennefeld M., 1993, A&A, 279, 53
Brandt W. N., Fabian A. C., Nandra K., Reynolds C. S., Brinkmann W., 1994, MNRAS, 271, 958
Celotti A., Fabian A. C., Rees M. J., 1992, MNRAS, 255, 419
Clavel J. et al., 1990, MNRAS, 246, 668
Clavel J. et al., 1991, ApJ, 366, 64
Clavel J. et al., 1992, ApJ, 393, 113
Courvoisier T. J.-L., Clavel J., 1991, A&A, 248, 389
Czerny B., Elvis M., 1987, ApJ, 321, 305

Downloaded from https://academic.oup.com/mnras/article/275/2/417/993736 by guest on 21 August 2022

© Royal Astronomical Society • Provided by the NASA Astrophysics Data System

1995MNRAS.275..417D

Czerny B., Zycki P., 1994, ApJ, 431, L5
Done C., Fabian A. C., 1989, MNRAS, 240, 81
Done C., Mulchaey J. S., Mushotzky R. F., Arnaud K. A., 1992, ApJ, 395, 275
Done C., Pounds K. A., Nandra K., Fabian A. C., 1994, in Gondhalekar P. M., Horne K., Peterson B. M., eds, ASP Conf. Ser. Vol. 69, Reverberation Mapping of the Broad Line Region in Active Galactic Nuclei. Astron. Soc. Pac., San Francisco, p. 211
Fabian A. C. et al., 1994, PASJ, 46, L59
Fiore F., Perola G. C., Matsuoka M., Yamauchi M., Piro L., 1992, A&A, 262, 37
Fiore F., Elvis M., McDowell J., Siemiginowska A., Wilkes B. J., 1994, ApJ, 431, 515
Frank J., King A. R., Raine D., 1992, in Accretion Power in Astrophysics, 2nd edition. Cambridge Univ. Press, Cambridge
George I., Fabian A. C., 1991, MNRAS, 249, 352
Gondhalekar P. M., Kellett B. J., Pounds K. A., Matthews L., Quenby J. J., 1994, MNRAS, 268, 973
Guilbert P. W., Rees M. J., 1988, MNRAS, 233, 475
Haardt F., Maraschi L., 1991, ApJ, 380, L51
Haardt F., Maraschi L., 1993, ApJ, 413, 507 (HM93)
Haardt F., Done C., Matt G., Fabian A. C., 1993, ApJ, 411, L95
Kallman T. R., Krolik J. H., 1987, ApJ, 320, L5
Krolik J. H., Begelman M. C., 1986, ApJ, 308, L55
Krolik J. H., Kriss G. A., 1995, ApJ, in press
Krolik J. H., Horne K., Kallman T. R., Malkan M. A., Edelson R. A., Kriss G. A., 1991, ApJ, 371, 541
Laor A., 1990, MNRAS, 246, 369
Lightman A. P., White T. R., 1988, ApJ, 335, 57
Matt G., Fabian A. C., Ross R., 1993, MNRAS, 264, 839
Mushotzky R. F., Done C., Pounds K. A., 1993, ARA&A, 31, 717
Nandra K., Pounds K. A., 1992, Nat, 359, 215
Nandra K., Pounds K. A., 1994, MNRAS, 268, 405 (NP94)
Nandra K., Pounds K. A., Stewart G. C., George I. M., Hayashida K., Makino F., Ohashi T., 1991, MNRAS, 248, 760
Nandra K. et al., 1993, MNRAS, 260, 504
Netzer H., 1993, ApJ, 411, 594
Osborne J., 1993, *ROSAT* UK Newsletter, No. 6, 7
Piro L., Yamauchi M., Matsuoka M., 1990, ApJ, 360, L35
Pounds K. A., 1995, in Makino F., Ohasi T., New Horizons of X-ray Astronomy. Universal Academy Press, Tokyo, Japan, p. 293
Pounds K. A., Nandra K., Stewart G. C., George I. M., Fabian A. C., 1990, Nat, 344, 132
Puchnarewicz E. M., Mason K. O., Cordova F. A., Kartje J., Branduardi-Raymont G., Mittaz J. P. D., Murdin P. G., Allington-Smith J., 1992, MNRAS, 256, 589
Reichert G. et al., 1994, ApJ, 425, 582
Ross R., Fabian A. C., 1993, MNRAS, 261, 74
Ross R., Fabian A. C., Minishige S., 1992, MNRAS, 258, 189
Rybiki G. B., Lightman A. P., 1979, Radiative Processes in Astrophysics. Wiley, New York
Shafer R. A., Haberl F., Arnaud K. A., Tennant A. F., 1991, XSPEC Users Guide, ESA TM-09
Shakura N., Sunyaev R., 1973, A&A, 24, 337
Turner T. J., 1993, OGIP calibration Note, CAL/ROS/93-007
Ueda Y., Ebisawa K., Done C., 1994, PASJ, 46, 107
Zdziarski A. A., Fabian A. C., Nandra K., Celotti A., Rees M. J., Done C., Coppi P. S., Madejski G. M., 1994, MNRAS, 269, L55
Zdziarski A. A., Johnson W. N., Done C., Smith D. A., McNaron-Brown K., 1995, ApJ, in press
Zycki P., Czerny B., 1994, MNRAS, 266, 653

Downloaded from https://academic.oup.com/mnras/article/275/2/417/993736 by guest on 21 August 2022

© Royal Astronomical Society • Provided by the NASA Astrophysics Data System